Association of Adhesive Spheres Formed by Hydrophobically End-Capped PEO. 1. Influence of the Presence of Single End-Capped PEO

Fabrice Laflèche, Dominique Durand, and Taco Nicolai*

Polymères, Colloïdes, Interfaces, UMR CNRS 6120, Université du Maine, 72085 Le Mans Cedex 9, France

Received July 8, 2002; Revised Manuscript Received November 7, 2002

ABSTRACT: Mixtures of poly(ethylene oxide) (PEO) end-capped on one or both ends with hexadecyl, but with the same hydrophilic−lypophilic balance, were studied using static and dynamic light scattering and dynamic mechanical measurements. In aqueous solution the mixtures form polymeric micelles with aggregation numbers that are independent of the fraction of difunctionalized PEO. Difunctionalized PEO bridges between two micelles, which leads to reversible association of the micelles. The phase behavior and the association of the micelles can be described by modeling the micelles as adhesive spheres with an adhesion parameter that depends on the fraction of difunctionalized PEO and the temperature. Above a given concentration the micelles percolate, leading to a strong increase of the viscosity and the high-frequency shear modulus. The viscosity has an Arrhenius temperature dependence with an activation energy close to that of the relaxation time that characterizes the decay of the shear modulus. At even higher concentrations an abrupt transition is observed that is characterized by the appearance of a second relaxation process with a very long relaxation time. The transition can be induced by small increases of the temperature or the concentration. The slow relaxation is attributed to restructuring of a solution of close packed micelles (e.g., hopping of micelles) while the fast relaxation, which is still visible at high concentrations, is attributed to the breakup of elastic bridges by the escape of end groups from the micelles.

Introduction

Associative polymers are polymers that contain functional groups that associate in selected good solvents for the polymer backbone. Telechelic associative polymers have the associating groups at the chain ends and are good model systems if they are monodisperse and well-characterized. A much investigated model system is poly(ethylene oxide) (PEO) with alkyl end groups in water.[1−12] Above a critical association concentration (cac) the end groups associate in multiplets, forming flowerlike polymeric micelles. Bridging between the micelles causes an effective attractive interaction which leads to reversible aggregation of the micelles. When the concentration is increased, the aggregates percolate and form a stable transient gel which induces a strong increase of the viscosity. At still higher concentrations the multiplets may form a more or less ordered liquid crystalline cubic phase, depending on the length of the PEO chains and the hydrophobicity of the end groups. This phase appears also for polymeric micelles obtained from polymers containing a single hydrophobic part. The rheology of such systems is characterized by a sudden transition to a so-called hard gel which does not flow.[13]

In some cases phase separation occurs into a dense transient gel phase at the bottom and a dilute top phase containing individual micelles and free chains.[1,4,5,11] Phase separation is induced by the entropy gain when end groups can exchange between more than one multiplet.[14] It is opposed by the loss of translational entropy of the micelles and the increase of excluded-volume interaction between overlapping PEO chains. Phase separation of PEO end-capped with alkyl groups via a urethane link (HEUR) was studied as a function of the temperature by Pham et al.[11] They used a model of adhesive hard spheres to obtain a quantitative description of the phase diagram.

Figure 1. Schematic drawings of polymeric micelles formed from monofunctionalized ($f = 0$) or difunctionalized ($f = 1$) polymers and a mixture of equal mass ratio ($f = 0.5$).

Phase separation can sometimes be avoided by addition of a small amount of surfactant,[1,15] but at the same time the properties of the micelles are modified. We will show that the same effect can be achieved in a controlled manner by addition of monofunctionalized PEO with half the molar mass, i.e., with the same hydrophilic−lipophilic balance (HLB). Monofunctionalized PEO forms micelles similar to starlike polymers.[10] The difference with micelles formed by double end-capped polymers with the same HLB is the absence of backfolding and bridging. Pictorially, micelles of monofunctionalized PEO are obtained by cutting the difunctionalized chains of the flowerlike micelles in two (see Figure 1). In homogeneous mixtures of mono- and difunctionalized chains each micelle contains both polymers with on average the same ratio as the total system, because that maximizes the mixing entropy. By varying the fraction (f) of difunctionalized PEO, we can vary the attraction between the micelles in a controlled manner and study its influence on the association of the micelles.

Here we present a study of PEO end-capped with hexadecyl using static and dynamic light scattering and rheology. The molar mass was 5 kg/mol for monofunctionalized PEO and 10 kg/mol for difunctionalized PEO, so that the HLB is the same. The effect of the alkyl length and chain backbone architecture will be presented in the accompanying paper. The experimental

10.1021/ma021076d CCC: $25.00
Published on Web 01/30/2003

results will be interpreted in terms of a mean field model, which we present in the following section.

Theory

We propose a simple mean-field model to calculate the phase diagram and the osmotic modulus of mixtures of single and double end-capped polymers. The main assumptions of the model are the following: (1) The functionalized polymers form polymeric micelles above a small critical association concentration. (2) The number of end groups (p) in the multiplet, i.e., the core of the micelles, does not depend on the polymer concentration or on the fraction of end groups from difunctionalized chains (f). (3) The free energy of mixing of the micelles contains only two terms: $F = F_a + F_b$. F_a is the free energy of mixing of polymer micelles without the effect of bridging. In good solvents F_a is positive and increases with increasing micelle concentration. F_b represents the gain in entropy if the end groups can exchange between different multiplets and becomes increasingly negative with increasing concentration. We neglect any concentration dependence of the internal free energy of the micelles.

F_a is the only contribution to the free energy of mixing for monofunctionalized polymers, and we expect that it does not depend on f. Star polymers with many arms and thus micelles made from monofunctionalized polymers with large aggregation numbers behave in good solvents like hard spheres for volume fractions (φ) below that of close packing.[16,17] For hard spheres the free energy of mixing per unit of volume is given by[18]

$$F_a = \frac{kT\varphi}{v}\left[\ln \varphi + \varphi \frac{4 - 3\varphi}{(1 - \varphi)^2}\right] \quad (1)$$

where v is the volume of a micelle. Here it is assumed that v does not depend on φ.

F_b can be estimated as follows using a mean-field approach. If two micelles are in contact, a number of end groups per micelle may exchange between the two multiplets and the system gains entropy.[14] The gain in entropy is k ln 2 per chain that can bridge, with k Boltzmann's constant. In principle, more micelles can be in contact simultaneously in such a way that an end group can exchange between more than two multiplets, but for this to happen the micelles need to interpenetrate strongly, which is unlikely for $\varphi < 1$.

The number of bridges that can be formed between two micelles in contact is proportional to p, and we can roughly estimate this number by assuming that at $\varphi = 1$ all difunctional chains can bridge. As each difunctional chain bridges two micelles, the maximum number of bridges per micelle is $^1/_2 fp$. Within the mean-field approach the number of micelles in contact is proportional to φ^2. The reduction of the free energy of mixing per unit of volume due to bridging is thus

$$F_b = -\frac{kT}{v} A\varphi^2 \quad (2)$$

where $A \approx {}^1/_2 \ln(2) fp$. Obviously this approach is not valid for φ close to and above unity.

Of course, polymeric micelles are not truly hard spheres. In addition, water is not an athermal solvent for PEO, and the solvent quality decreases with increasing temperature. This means that the excluded-volume interactions are smaller than for hard spheres. We will take this into account by using an effective volume fraction in the calculation of F_a:

$$\varphi_e = \varphi \frac{v_e(T)}{v} \quad (3)$$

Here $v_e(T)$ is the effective volume of the micelles and depends on the temperature. If we use this definition of φ, we need to replace the parameter A by an effective temperature-dependent value:

$$A \approx \frac{v}{v_e(T)} \frac{1}{2} \ln(2) fp \quad (4)$$

In view of the approximations the numerical prefactor in eq 4 is only a rough estimate. The binodal can be calculated using the points of contact with common tangent on $F(\varphi)$ to determine the volume fractions of the equilibrium phase.[19] The critical volume fraction is $\varphi_c = 0.13$, and the corresponding critical interaction parameter is $A_c = 10.6$.

To go beyond mean-field theory, higher-order interactions need to be considered. Baxter showed that the phase diagram and the structure factor of adhesive hard spheres can be calculated analytically using the Percus–Yevink approximation, when choosing a specific interaction potential that is characterized by a single parameter, τ.[20] Subsequently, computer simulations showed that this model also describes hard spheres interacting with a square well potential if the interaction range is small compared to the size of the particles.[21] The interaction parameter τ is related to the range and the depth of the square well. If we approximate the binary interaction between polymeric micelles with a short-range square well potential, the parameter A corresponds to τ^{-1} in Baxter's theory of sticky spheres. The critical values of this model are almost the same: $\varphi_c = 0.121$ and $A_c = 10.2$.

Materials and Methods

Materials. Commercial PEO samples with nominal molar mass 5 kg/mol containing a hydroxyl group at one end (P5000) and with nominal mass 10 kg/mol containing hydroxyl groups on both ends (P10000) were purchased from Fluka. The samples were characterized using size exclusion chromatography (SEC) and light scattering. SEC in THF showed that P5000 contained 20% (w/w) difunctionalized PEO chains with double the molar mass probably due to the presence of trace water during the synthesis. The ratio of the weight- and number-average molar mass (M_w/M_n) is less than 1.1 for both fractions. P10000 is unpolluted and again $M_w/M_n < 1.1$. From static light scattering experiments we obtained $M_w = 6.0$ kg/mol for P5000 and $M_w = 9.8$ kg/mol for P10000. From the fact that P5000 contains 20% material with double the molar mass it follows that M_w of the monofunctionalized fraction is 5.0 kg/mol. The z-average hydrodynamic radii of the samples were obtained from dynamic light scattering experiments: $R_h = 2.5$ nm for P5000 and $R_h = 3.2$ nm for P10000. Considering again that P5000 contains 20% material with double the molar mass and thus $R_h = 3.2$ nm, we find $R_h = 2.25$ nm for the monofunctionalized fraction.

The samples were functionalized by reaction of the terminal hydroxyl groups with hexadecylchloric acid. The latter was obtain by solubilizing commercial hexadecyl acid (Aldrich) in $SOCl_2$ and stirring it under reflux at 80 °C overnight. The excess of $SOCl_2$ was eliminated by cryodistillation. POE and hexadecylchloric acid were dissolved in water-free dichloromethane. A large excess of the hexadecylchloric acid solution was added dropwise to the POE solution. The mixture was stirred under reflux at 40 °C for 2 h, after which a large excess of $NaHCO_3$ was added at room temperature which leads to

precipitation of the excess hexadecylchloric acid. The mixture was filtered, and the modified POE was purified by repeated precipitation in pentane. The degree of functionalization was found with NMR to be 100% within an experimental error of about 5%. SEC of the samples in THF showed no difference before and after functionalization.

Sample Preparation. Functionalized PEO was dissolved in Milli-Q water and homogenized by slowly turning the samples. For light scattering measurements the samples were filtered through 0.2 μm pore size Anatop filters when possible. Viscous samples were filtered through 0.45 μm pore size Millipore filters. We checked that filtration did not modify the concentration.

Methods. Dynamic mechanical measurements were done on a stress-controlled rheometer (AR1000, TA Instruments) using a cone−plate geometry. The temperature was controlled using a Peltier system. Care was taken to avoid solvent evaporation. The stress was chosen low enough to measure a linear viscoelastic response.

Light scattering measurements were made using an ALV-5000 multibit, multitau, full digital correlator in combination with a Spectra-Physics laser emitting vertically polarized light at $\lambda = 532$ nm. The temperature was controlled by a thermostat bath to within ±0.1 °C. We have used a toluene standard with Rayleigh ratio 2.79×10^{-5} cm^{-1} at $\lambda = 532$ nm and 20 °C.[22] The refractive index increment of modified and unmodified PEO is 0.14 mL/g.[23] The autocorrelation functions were analyzed in terms of a relaxation time (τ) distribution (see ref 9). In all cases a q^2-dependent mode was observed, and the cooperative diffusion coefficient was calculated from the average relaxation rate as $D_c = \langle\tau^{-1}\rangle/q^2$.[24] At higher concentrations additional slow modes were observed in which case we used the fast mode to calculate D_c.

Observation of Phase Separation. To observe the phase behavior, samples were put in a thermostated oil bath. Phase separation was characterized by the appearance of a clear top phase and a turbid, viscous bottom phase. The height of the bottom phase decreased slowly with time until it settled to a stable value. During this period the turbidity of the bottom phase decreased. The reproducibility of the final height of the bottom phase was checked by rehomogenization of the sample. Contrary to the results reported by Pham et al.,[12] we observed a variation of the height when varying the temperature. However, this variation establishes itself very slowly and is only clearly observed if the samples are homogenized at each temperature.

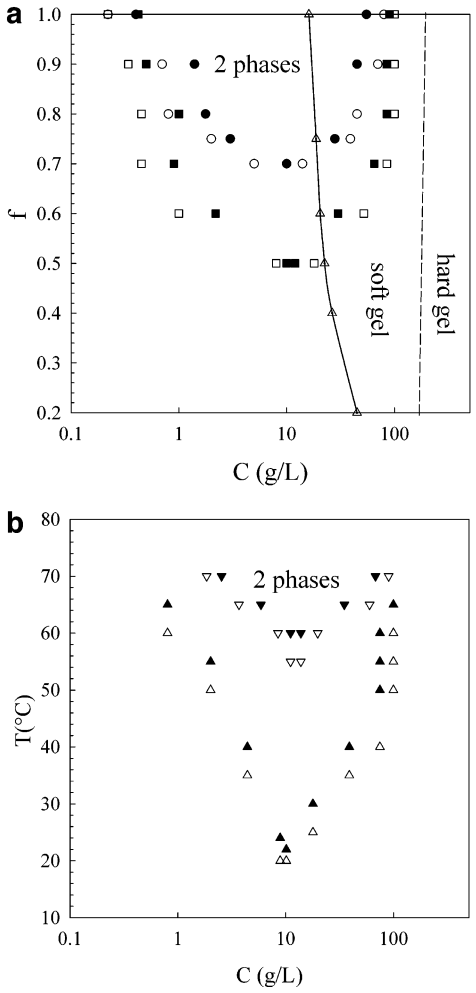

Figure 2. Phase diagrams of mixtures of mono- and difunctionalized PEO. (a) shows the $f-C$ phase diagrams at 20 °C (○) and 60 °C (□), and (b) shows the $T-C$ phase diagrams at $f = 0.5$ (▽) and $f = 0.7$ (△). The open symbols represent homogeneous samples, and the filled symbols represent phase-separated samples. The triangles in (a) represent the percolation threshold (C_p), while the dashed line indicates the transition to the so-called hard gel (see text).

Results

Phase Behavior. We observed a large number of mixtures of monofunctionalized PEO with $M_w = 5$ kg/mol and difunctionalized PEO with $M_w = 10$ kg/mol over a range of f and T. The fraction of difunctionalized PEO in the sample P5000 was taken into account in the calculation of f. The samples were functionalized with hexadecyl (C16). Some samples phase separated slowly into a gellike bottom phase and a liquid top phase. Figure 2a shows the $f-C$ phase diagram at two temperatures, while Figure 2b shows the $T-C$ phase diagram at two values of f. At low concentrations the volume fraction of the dense phase is very small, and it is difficult to establish with high precision the border between homogeneous and phase-separated samples. The critical concentration (C_c) is the position of the minimum and is in all cases between 10 and 15 g/L.

For purely difunctionalized PEO the amount of PEO in the top phase is negligible, and the height of the bottom phase is proportional to the total PEO concentration. However, for mixtures of mono- and difunctionalized PEO the concentration of the top phase increased when we increased the total PEO concentration. This means that the tie lines are slanted, and the repartition of mono- and difunctionalized PEO is different in the two phases. As mentioned above, in the homogeneous phase one expects that the repartition is about the same in each micelle because that maximizes the entropy. However, for phase-separated samples micelles can escape to the dilute phase if they have a lower fraction of difunctional PEO. The reduction of the mixing entropy within the micelles is compensated by a gain in translation entropy of the micelles. Therefore, phase separation in mixtures leads to fractionation.

We measured the scattered light intensity as a function of the temperature of mixtures at $C = 10$ g/L, i.e., approximately C_c, with varying f. The intensity diverges at the so-called cloud point temperature which depends on f (see Figure 3). Figure 3 shows how much monofunctionalized PEO needs to be added to obtain a homogeneous solution over the whole concentration range.

Static Light Scattering. We measured the scattering intensity of mixtures over a range of concentrations at different values of f and T. Unfiltered solutions show a contribution of spurious scattering due to the presence of a small weight fraction of aggregated material. Their presence leads to an additional slow relaxation mode

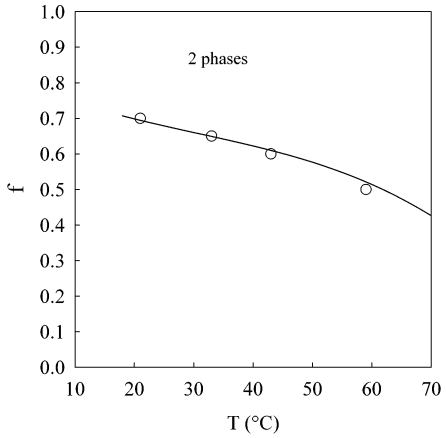

Figure 3. $f-T$ phase diagram of mixtures of mono- and difunctionalized PEO close to the critical concentration. The solid line represents the theoretical prediction $f \propto v_e(T)$ (see text).

of the autocorrelation function of the scattered light. For dilute solutions the aggregates can be removed by careful filtration through 0.2 μm filters. However, the viscosity of the samples increases with increasing concentration, and it becomes increasingly difficult to filter out all the spurious scatterers. Therefore, we have corrected the scattering intensity using dynamic light scattering results. We have multiplied the relative amplitude of the fast mode with the total scattering intensity in order to obtain the scattering intensity of just the fast mode (I) and used this value to calculate the relative excess scattering $I_r = (I - I_{sol})/I_{tol}$. See ref 9 for more details of the analysis method. The relative amplitude of the fast mode varied between 10% and 100%, with the lowest value obtained for the most viscous samples.

It is clear that this procedure adds to the experimental error and limits the range of concentrations that can be explored with light scattering. Although the presence of aggregates in aqueous PEO solutions is well-known, it is not the only reason for the appearance of slow modes in the autocorrelation function. Slow modes unrelated to spurious aggregates have been observed in concentrated solutions of star polymers[25] and in most gels including transient gels formed by telechelic polymers.[26,27] However, we are not able to distinguish well between the different possible origins of the slow modes and do not pursue this matter here.

In Figure 4a we have plotted the concentration dependence of KC/I_r at 20 °C for mixtures at different values of f. K is a constant given by[28]

$$K = \frac{4\pi^2 n^2}{\lambda^4 N_a}\left(\frac{\partial n}{\partial C}\right)^2\left(\frac{n_s}{n}\right)^2\frac{1}{R_s} \qquad (5)$$

where N_a is Avogadro's number, λ is the wavelength of the incident light, $(\partial n/\partial C)$is the refractive index increment, and R_s is the Rayleigh ratio of the standard. $(n_s/n)^2$ corrects for the difference in scattering volume of the solution with refractive index n and the standard with refractive index n_s. The dependence on the scattering wave vector (q) was negligible in all cases. I_r is proportional to the osmotic compressibility:[28]

$$KC/I_r = (\mathrm{d}\pi/\mathrm{d}C)/RT \qquad (6)$$

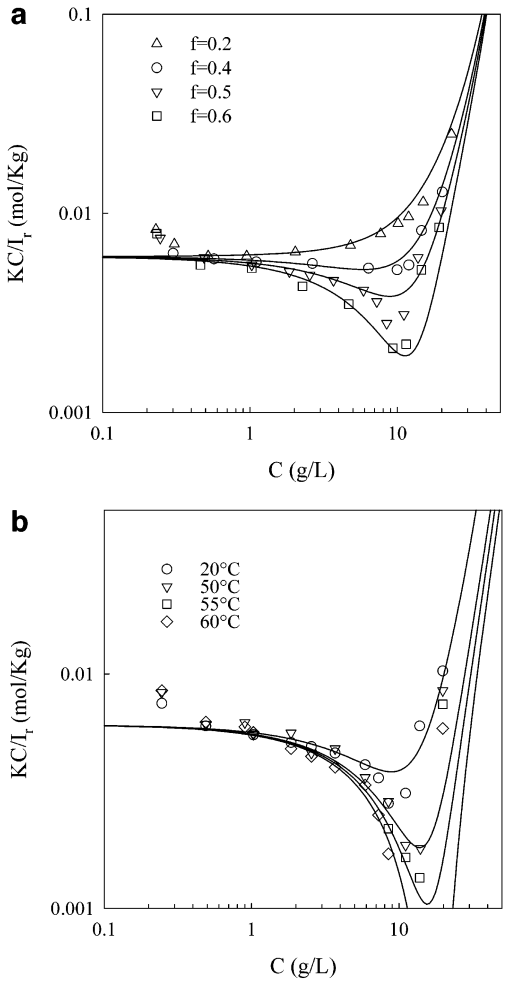

Figure 4. Concentration dependence of KC/I_r at $T = 20$ °C for different values of f (a) and at $f = 0.5$ for different temperatures (b). The solid lines are model predictions (see text).

with R the gas constant and T the absolute temperature. At low concentrations interactions may be neglected, and $KC/I_r = 1/M_w$.

For these samples the cac is low and cannot be determined with light scattering. But at the lowest concentrations the contribution of free chains to the scattering intensity is no longer negligible. Their contribution causes the upturn of KC/I_r with decreasing concentration at the low concentration end. It is clear that M_w of the micelles does not vary with f, which means that the number of end groups per micelle ($p = 33$) does not depend on the functionality of the chains as long as they have the same HLB. For larger values of f, KC/I_r decreases with increasing concentration until it reaches a minimum at $C \approx 10$ g/L, after which it increases again. The decrease is caused by the bridging of the micelles while the subsequent increase is due to excluded-volume interactions between the micelles. The minimum becomes more pronounced with increasing f and diverges at the critical value $f_c = 0.7$. At higher values of f the system phase separates (see Figure 2a).

Figure 4b shows the results for $f = 0.5$ at different temperatures. Again we observe very little variation at low concentrations, which means that the aggregation number is independent of the temperature. The effect of temperature is thus caused by the variation of $v_e(T)$, i.e., the thermodynamic volume of the micelles. The minimum becomes more pronounced with increasing

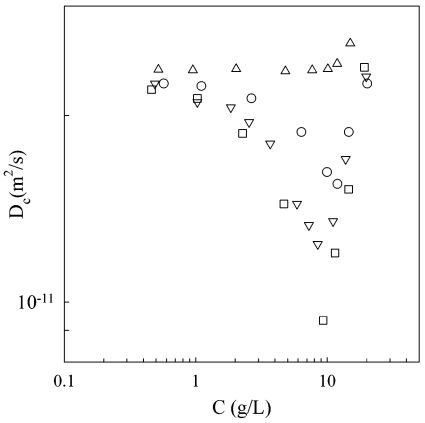

Figure 5. Concentration dependence of the cooperative diffusion coefficient at $T = 20$ °C for different values of f. Symbols are as in Figure 4a.

temperature and diverges at the critical temperature $T_c = 58$ °C.

Dynamic Light Scattering. Figure 5 shows the concentration dependence of the cooperative diffusion coefficient. We may write D_c in terms of the osmotic compressibility modulus and a friction coefficient (f_r) that increases with the concentration:[24]

$$D_c = \frac{(1 - \rho/C)^2}{f_r}\frac{d\pi}{dC} \tag{7}$$

where ρ is the density of the solute. The concentration dependence of D_c is consistent with the static light scattering results, but lacking an expression for f_r we cannot give a quantitative analysis.

At low concentrations where the interaction between micelles is negligible D_c becomes equal to the self-diffusion coefficient (D_s), and we may use the Stokes−Einstein equation to calculated the z-average hydrodynamic radius of the micelles (R_h):

$$D_s = \frac{kT}{6\pi\eta R_{hz}} \tag{8}$$

with η the viscosity. We find that $R_h = 9.3$ nm independent of f and T.

Dynamic Mechanical Measurements. We have measured the radial frequency (ω) dependence of the loss (G'') and storage (G') shear modulus over a range of concentrations at different values of f and T. The results at different temperatures between 10 and 40 °C could be superimposed by simple frequency shifts. Figure 6 shows results of time−temperature superpositions with $T_{ref} = 20$ °C at $C = 100$ g/L for three values of f. The mechanical relaxation is characterized by a narrow relaxation process, and at high frequencies the system behaves as a gel. This behavior is typical for telechelic associative polymers,[3,27] and the terminal relaxation process is generally assumed to be controlled by the average escape time of an end group from the multiplet. However, for $f = 0.75$ and 1 we observed a shoulder at low frequencies, which became more important with increasing concentration. We have determined the relaxation time from the maximum in G'', $\tau_r = 1/\omega_{max}$, and estimated the gel modulus (G_0) from G' at high frequencies.

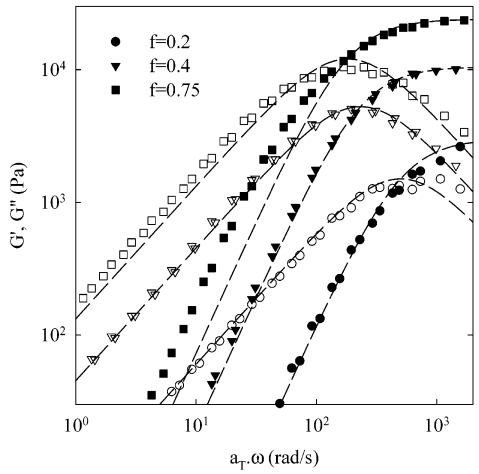

Figure 6. Master curves of the angular frequency dependence of the loss (open symbols) and storage (filled symbols) shear modulus at different values of f for $C = 100$ g/L and $T_{ref} = 20$ °C. The dashed lines represent the dependence for a single relaxation time.

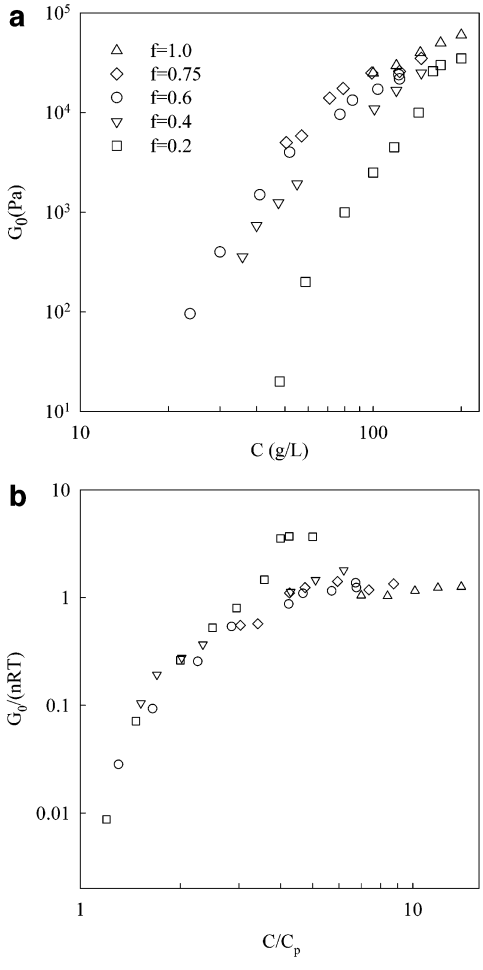

Figure 7. (a) shows the concentration dependence of the gel modulus at 20 °C for different values of f indicated in the figure. (b) shows the same data after normalization of G_0 with nRT and C with C_p. At the highest concentration for $f = 1.0$ and the highest three concentrations for $f = 0.2$ the system formed a so-called hard gel.

Figure 7a shows the concentration dependence of G_0 for different values of f. G_0 strongly increases with increasing C above a given concentration C_p that decreases with increasing f. C_p may be considered as the percolation threshold beyond which a transient gel

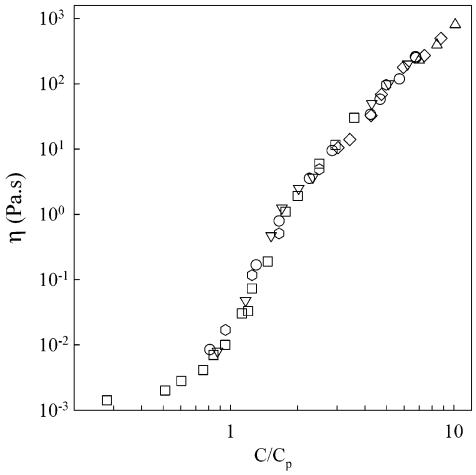

Figure 8. Normalized concentration dependence of the viscosity at 20 °C for different values of *f*. The symbols are as in Figure 7a.

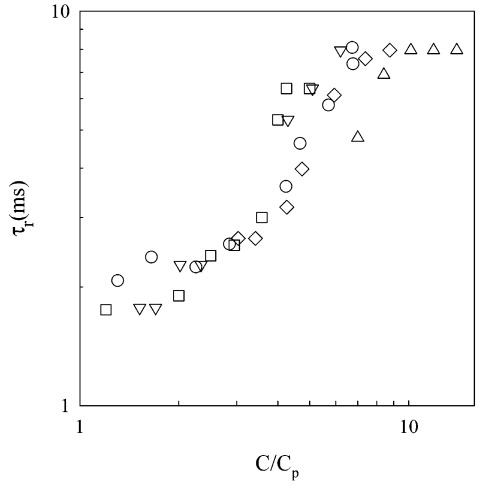

Figure 9. Normalized concentration dependence of the relaxation time at 20 °C for different values of *f*. The symbols are as in Figure 7a.

is formed. For $f = 1$ and 0.75 phase separation limits the range of concentrations that can be explored. For polymeric gels the elastic modulus is proportional to the molar concentration of elastically active network chains (ν): $G_0 = a\nu RT$, with R the gas constant.[29] The prefactor a is unity for affine deformation, while for nonaffine deformation it is less depending on the cross-link functionality, but it is still close to unity for highly functionalized cross-links. The total molar concentration of difunctionalized chains is $n = fC/M_n$, with M_n the molar mass of the difunctionalized chains. The fraction that is elastically active is equal to $\nu/n = G_0/(nRT)$. We have plotted in Figure 7b $G_0/(nRT)$ as a function of C/C_p. Of course, the absolute value of C_p is not very well-defined, but the relative variation of C_p with f can be obtained quite accurately by this superposition and that of the viscosity. The values of C_p used in the superposition are 45, 27, 23, 21, 19, and 16 g/L for $f = 0.2$, 0.4, 0.5, 0.6, 0.75, and 1, respectively. The concentration dependence of C_p is plotted in Figure 2a. For $f = 1$ the accessible concentration range is very small, and C_p is only indicative. ν/n increases rapidly above C_p and stabilizes at a value close to unity for $C > 3C_p$ if f is large. However, if f is small it reaches values above unity caused by an additional contribution to the shear modulus (see below).

Figure 8 shows that the concentration dependence of the viscosity at 20 °C for different f also superimposes if we plot the results as a function of C/C_p with the same values for C_p. At C_p the viscosity rises steeply followed by a weaker increase at higher concentrations. The concentration dependence of the viscosity is essentially due to that of the elastic modulus, because the concentration dependence of the relaxation time is relatively weak (see Figure 9). The viscosity increases with decreasing temperature following an Arrhenius temperature dependence with activation energy $E_a = 73$ kJ/mol independent of f. This value is close to that reported by Annable et al. (71 kJ/mol) for PEO end-capped with C16 via a urethane link.[3] The temperature dependence of τ_r is characterized by the same activation energy as for η, because G_0 is independent of the temperature.

If we increase the PEO concentration further, a transition occurs to a different rheological behavior. The transition is strongly temperature dependent and is illustrated in Figure 10. A small increase of the concentration or decrease of the temperature leads to a very large increase of the terminal relaxation time. The relaxation process caused by the escape of the end groups from the multiplet is still clearly visible, but this no longer leads to full relaxation of the stress. The transition is not immediate after a decrease of the temperature but appears progressively over a period of time. We assimilate this phenomenon with the transi-

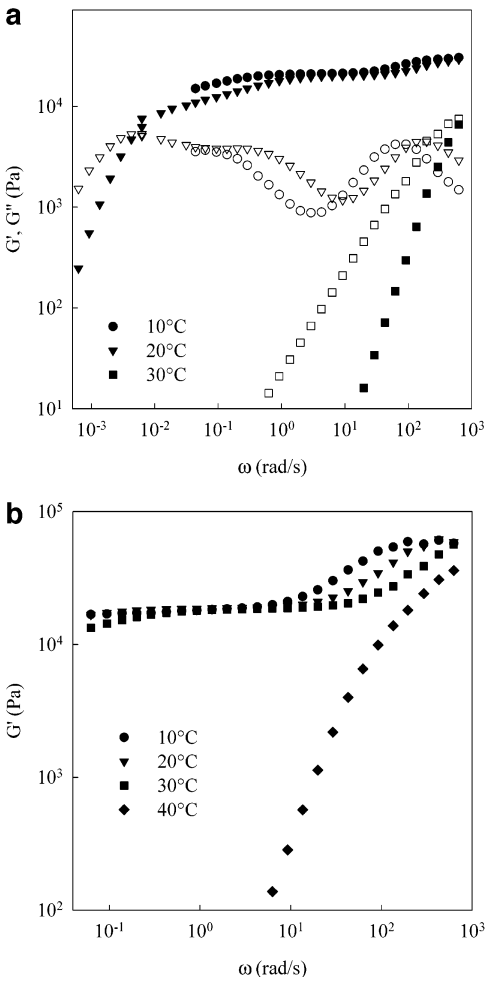

Figure 10. Angular frequency dependence of the loss (open symbols) and storage (filled symbols) shear modulus at different temperatures. (a) shows the data for $C = 170$ g/L and $f = 0.2$, and (b) shows the data for $C = 200$ g/L and $f = 1.0$. For clarity, G'' is not shown in (b).

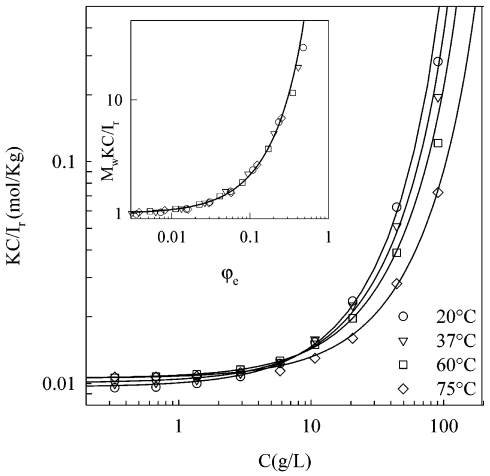

Figure 11. Concentration dependence of KC/I_r for Brij700 at different temperatures. The inset shows the same data in a reduced representation.

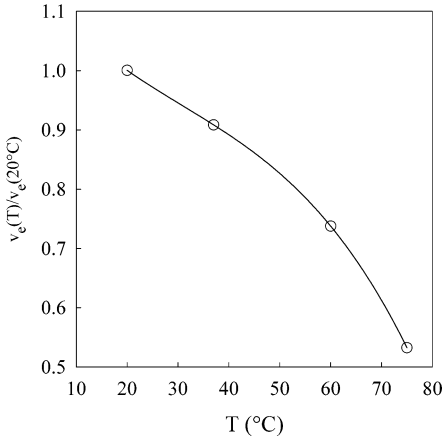

Figure 12. Temperature dependence of the effective volume of Brij700 relative to the value at 20 °C. The solid line is a guide to the eye.

tion between a liquid and a so-called hard gel that does not flow when tilted, which is reported for star polymers[25] and diblock copolymers.[14] With increasing concentration the transition occurs at higher temperatures; e.g., for $f = 0.2$ it occurs below 10 °C at 118 g/L, between 10 and 20 °C at 143 g/L, between 20 and 30 °C at 170 g/L, and between 30 and 40 °C at 200 g/L. However, the transition depends only weakly on f: for $f = 1$ the transition occurs between 20 and 30 °C at 200 g/L. The modulus of the hard gel, i.e., at low frequencies, is about the same at $f = 0.2$ and $f = 1$, but the high-frequency modulus is larger for $f = 1$. The relative contribution of the hard gel modulus at high frequencies is important for $f = 0.2$, which explains why the calculated value of ν/n is significantly larger than unity.

Discussion

Thermodynamics. To compare the experimental results to the theory presented above, we need to relate the parameters f and T to A. The relation between f and A is straightforward, but the relation between A and T needs to be established. For that purpose we have studied a commercial sample Brij700 (Aldrich) over a range of concentrations at different temperatures. Brij700 is a PEO with molar mass 4 kg/mol end-capped with C18, and it is 100% monofunctional. There is therefore no effect of bridging on the interactions between the micelles, i.e., $A = 0$. Static light scattering results are shown in Figure 11. Again we observed almost no effect of temperature on the number of hydrophobic groups per micelles ($p = 26$). Similarly, DLS showed no significant variation of R_h with T ($R_h = 7.6$ nm).

The inverse osmotic compressibility is related to the free energy of mixing as[19]

$$\frac{d\pi}{dC} = C\frac{d^2F}{dC^2} \tag{9}$$

Using eqs 1, 2, 6 and 9 and expressing the effective volume fraction as $\varphi_e = C/C_s$ with $C_s = M_w/(N_a v_e(T))$, we obtain

$$\frac{KC}{I_r} = \frac{1}{M_w}\left[\frac{1 + 4\varphi_e + 4\varphi_e^2 - 4\varphi_e^3 + \varphi_e^4}{(1-\varphi_e)^4} - 2A\varphi_e\right] \tag{10}$$

The solid lines in Figure 11 are fits to eq 10 with $A = 0$ and give a good description of the data. The inset shows the collapse of the data if we plot M_wKC/I_r as a function of φ_e. From the temperature dependence of C_s we calculated the relative variation of $v_e(T)$. The results are plotted in Figure 12. Although the commercial sample is different from the samples, we have studied here the relative variation of $v_e(T)$ for Brij700 is probably a good approximation for the other samples.

We can compare the light scattering results at different f and T with the model using eq 10. Because p and v are independent of f and T, we can use $A = bf/v_e(T)$, where b is a proportionality constant. Séréro et al.[10] compared mono- and difunctionalized PEO with the same molar mass as the samples studied here, but with partially perfluorinated alkyl end groups. These end groups are more hydrophobic, and thus the value of p deduced from neutron scattering was higher. However, it was found to be the same for mono- and difunctionalized PEO ($p = 100$), in agreement with the present findings. They observed no concentration dependence up to 80 g/L.

The solid lines in Figure 4 are model predictions with $M_w = 165$ kg/mol ($p = 33$), $v_e(20\ °C) = 2.7 \times 10^3$ nm^3 ($C_s = 100$ g/L), and $b = 4.5 \times 10^4$ nm^3. We have chosen $v_e(20\ °C)$ to give the best description of the minimum of KC/I_r, since we have limited information about the increase of KC/I_r near C_s, which we expect in any case not to be properly described by the model. We can calculate the thermodynamic radius (R_T) at 20 °C using $v_e = {}^4/_3\pi R_T^3$ and compare it with the hydrodynamic radius which is almost temperature independent: $R_T = 8.6$ nm and $R_h = 9.3$ nm. As expected, $R_T < R_h$ and the difference increases with increasing temperature. The model predicts that b is approximately ${}^1/_2\ln(2)\nu p$. If we assume that $\nu = {}^4/_3\pi R_h^3$, we find $b = 3.7 \times 10^4$ nm^3, which is remarkably close to the value used to fit the experimental data.

We can compare the experimental phase diagrams with model predictions by plotting A/A_c vs φ_e/φ_c. A/A_c is equal to f/f_c for the $f-C$ phase diagrams and $v_e(T_c)/v_e(T)$ for the $T-C$ phase diagrams. To calculate $\varphi_e = C/C_s$, we have used $C_s = 100$ g/L at 20 °C obtained from the light scattering experiments. The value of C_s at other temperatures was calculated as $C_s(T) = C_s(20\ °C)\nu(T)/\nu(20\ °C)$ using the results for Brij700. For the critical volume fraction we used $\varphi_c = 0.1$. Figure 13 shows that the four phase diagrams of Figure 2 superimpose in this

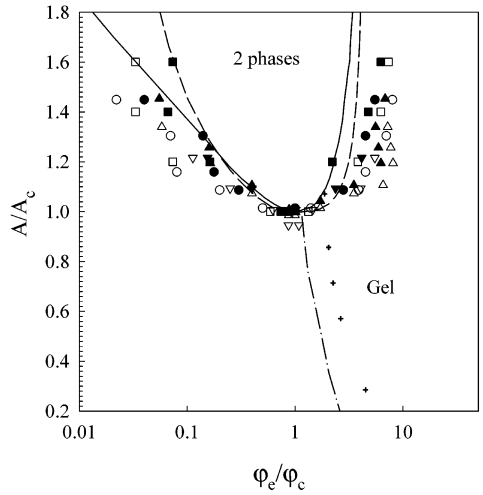

Figure 13. Normalized representation of the phase diagrams shown in Figure 2. The solid and dashed line represent the theoretical binodals obtained from the mean-field approach and the Baxter model, respectively (see text). The dashed−dotted line represents the percolation threshold found in computer simulations, and the crosses represent experimental values at 20 °C.

representation although with some considerable scatter. The solid and dashed lines in Figure 13 show the theoretical binodals for adhesive spheres using the mean-field approach and the Baxter model,[30] respectively (see Theory section). The two phase regime is broader than predicted by the theory, probably because higher-order excluded-volume interactions for polymeric micelles are weaker than for hard spheres.

From eq 4 it follows that $f_c \propto v_e(T_c)$ if p and v are independent of f and T. Figure 2 shows that this prediction is compatible with the experimental results. These results also give an independent estimate for the proportionality factor $b = 4.1 \times 10^4$ nm^3. In view of the gross simplifications of the model, exact agreement is not to be expected, but the semiquantitative agreement means that the model captures the essential features of the thermodynamic properties of the hydrophobically end-capped PEO that we investigated.

In this paper we have rationalized the concentration dependence of the scattered light intensity in terms of concentration fluctuations of individual micelles. In first instance this approach appears different from the one that we employed earlier.[9] In ref 9 the initial decrease of KC/I_r was attributed to an increase of M_w, i.e., association of the micelles, and the subsequent increase by excluded-volume interactions between associated micelles. But, because the association is reversible, the distinction between concentration fluctuations of individual micelles and transient associations is merely one of terminology. Formally, one can equally well include the attractive interaction in eq 10 via a concentration-dependent molar mass. Of course, the difficulty then is first to describe the concentration dependence of the molar mass distribution of the associated micelles and second to describe the excluded-volume interactions between the associated micelles. We described the association using the open association model where the equilibrium constant depends on p and f. Furthermore, we assumed that the excluded-volume interactions were the same as for individual PEO chains at least at higher concentrations. The latter assumption is clearly wrong in the present case of micelles made of short PEO chains but may be closer to reality if larger PEO chains are used. Qualitatively, the concentration dependence of KC/I_r could be described quite well, but for a more quantitative description computer simulations of the reversible association process are required.

Pham et al.[11] also used a model of adhesive hard spheres to explain the phase behavior of hydrophobically end-capped PEO. They used the binary interaction potential between two micelles proposed by Semenov et al.[14] to calculate the value of A. However, this calculation led to values of A that were much too large.

It is clear that adding monofunctionalized PEO to difunctionalized PEO with the same HLB should always reduce the tendency to phase separation. However, Alami et al.[8] reported that addition of a small fraction of neutral surfactant to difunctionalized PEO leads to a decrease of the phase separation temperature. When the fraction of the surfactant is increased, the phase separation temperature increases again. The effect of adding surfactants on the phase behavior is generally difficult to interpret, because it influences both p and the excluded-volume interactions. For the specific system studied by Alami et al., the authors mention that the micelles could contain more difunctionalized PEO after addition of a small fraction of surfactant, which would favor phase separation.

Rheology. As mentioned above, the strong rise of the viscosity is caused by the formation of a transient network. Bridging leads to reversible aggregation of the polymeric micelles. With increasing concentration larger clusters are formed until they percolate the system at C_p. For irreversible bonds this leads to divergence of the viscosity and the appearance of an elastic modulus at low frequencies. In the present case the bonds have a finite lifetime which is controlled by the escape time of the end groups from the multiplet and is independent of f. Therefore, the elastic modulus is only observed at high frequencies.

For adhesive hard spheres the percolation threshold has been calculated using computer simulations[31] (see the dashed−dotted line in Figure 13). We cannot compare the simulation results directly with the experimental results because for a given value of f, $v_e(T)$ and thus φ_e depend on the temperature, while C_p is insensitive to the temperature and depends on v. However, there is a semiquantitative agreement with the experimental results at 20 °C, especially if we consider that $v_e(T)$ is somewhat smaller than v. The question arises whether the continuation of the percolation threshold in the two phase region has a physical significance. Recent computer simulations have shown that a temporary gel may be formed in the two phase regime with a lifetime that increases with increasing attractive interactions.[32] This could explain the slow phase separation that we observe after homogenizing systems in this temporary gel phase.

At the gel point the gel fraction is infinitely small, but it rises rapidly with increasing concentration. The gel fraction itself contains loops and dangling ends that are elastically inactive. Annable et al.[3] proposed a theory, backed up by Monte Carlo simulations, to calculate the fraction of elastically active network chains as a function of the concentration. However, for simplicity the authors assumed that the position of the micelles are uncorrelated which is wrong, because bridging micelles will be at a preferred distance independent of the total concentration. Qualitatively, the increase of

ν/n from 0 at C_p to unity at about $3C_p$ can be understood in terms of an increasing effective functionality of the micelles, but for a quantitative description more realistic computer simulations are required.

The terminal relaxation time increases with increasing PEO concentration. Close to C_p so-called super bridges[3] are formed, i.e., elastic network chains that contain more than one PEO chain. The escape of any chain end in the super bridge relaxes the stress which decreases τ_r. The fraction and the length of super bridges decrease with increasing concentration so that τ_r increases with C. Figure 9 shows that τ_r is approximately independent of f at a given value of C/C_p and thus a given value of $G_0/(nRT)$. This means that τ_r is mainly determined by the fraction of bridges that is elastically active.

At a fixed polymer concentration the viscosity decreases with decreasing f. However, at a fixed concentration of difunctional chains the viscosity actually increases with decreasing f. The increase of the volume fraction of polymeric micelles compensates for the reduction of the functionality of each micelle. For the same reason an increase of the viscosity is often observed if small surfactants are added to associative polymers.[1,33,34] Of course, in the latter case one also modifies the structure of the micelles; notably excluded-volume interactions between the micelles are reduced. If one continues to add small surfactants, the viscosity reaches a maximum and decreases with further addition. The reason is that at high concentrations of surfactants the reduction of the functionality dominates, and finally the micelles cease to percolate. For the present system this situation cannot be reached even for $f = 0.2$ because addition of a large fraction of monofunctionalized PEO leads to strong excluded-volume interactions between the micelles and the formation of a so-called hard gel.

At higher concentrations the micelles closely pack, and at a concentration $C_{hg} > C_p$ the system jams, which is characterized by the arrest of flow. C_{hg} is strongly temperature dependent, but it is almost independent of f. Jamming of the micelles is induced by excluded-volume interactions and is therefore controlled by the thermodynamic volume of micelles, which itself is almost independent of f. In fact, we have observed this transition also for Brij700, which cannot bridge at all. A temperature-dependent transition to a nonflowing gel phase has been observed for diblock copolymers[13] and star polymers.[25] In some cases the hard gel was preceded by a so-called soft gel which flows upon tube inversal. The soft gel was attributed to temperature-dependent attractive interactions between the micelles.[35,36] Lobry et al.[36] determined the phase diagram and the percolation threshold of a triblock copolymer with a hydrophobic middle block (Pluronic). They interpreted their results in terms of adhesive spheres in a manner similar to our interpretation. However, the attractive interaction between Pluronics is not well understood. The terminal relaxation time of the soft gel is very long for that system.

For the present system the origin of the attractive interactions is clear and can be quantified. In one case we have determined the frequency dependence of G'' down to very low frequencies (see Figure 10a). For this system we observe the relaxation of the hard gel well separated from that of the bridges. The relaxation of the hard gel might be due to hopping or complete restructuration of the micelles. We will present a more detailed study of the transition to a hard gel elsewhere.

The results presented here show similarities with those obtained for suspensions of stabilized oil droplets in the presence of difunctionalized PEO.[37] For this system phase separation is induced above of a critical number of difunctionalized PEO chains per droplet. They also observed slanted tie lines because the system can gain entropy if the droplets in the dense phase contain more difunctionalized PEO than those in the dilute phase. The binodal should nevertheless be the same as for adhesive spheres unless there is a distribution in the number of difunctionalized chains per droplet already in the homogeneous phase. In the homogeneous phase they also observed the formation of a transient gel at a percolation concentration that increased with decreasing PEO concentration.

Conclusion

Hydrophobically end-capped PEO forms polymeric micelles in aqueous solution with a number of hydrophobic groups per micelles that is independent of the ratio of mono- and difunctionalized chains if the HLB is kept the same. Increasing the temperature reduces exclude-volume interaction between the micelles, but their molar mass and hydrodynamic radius change very little.

The micelles phase separate above a critical temperature that decreases with increasing fraction of difunctional chains. The system can be modeled as a collection of adhesive spheres with an adhesion parameter that is proportional to the number of difunctionalized chains per micelle and inversely proportional to the thermodynamic volume of the micelles. This model describes semiquantitatively the phase diagrams and the concentration dependence of the osmotic compressibility.

The mechanical properties can be interpreted in terms of the formation of a transient network of bridging micelles. The terminal relaxation time is determined by the escape time of an end group from the multiplet which is independent of the fraction of difunctionalized chains. The elastic modulus has a very weak temperature dependence, and both the terminal relaxation time and the viscosity have an Arrhenius temperature dependence.

At a higher concentration the system shows a transition to a nonflowing gel that is caused by jamming of closely packed micelles. This transition is strongly temperature dependent but almost independent of the fraction of difunctionalized chains.

References and Notes

(1) Kaczmarski, J. P.; Glass, J. E. *Macromolecules* **1993**, *26*, 5149.
(2) Yekta, A.; Xu, B.; Duhamel, J.; Adiwidjaja, H.; Winnik, M. A. *Macromolecules* **1995**, *28*, 956.
(3) Annable, T.; Buscall, R.; Ettelai, R.; Whittlestone, D. *J. Rheol.* **1993**, *37*, 695.
(4) Alami, E. Rawiso, M.; Isel, F.; Beinert, G.; Binane-Limbele, W.; François, J. *ACS Adv. Chem.* **1996**, *248*, 343.
(5) François, J.; Maitre, S.; Rawiso, M.; Sarazin, D.; Beinert, G.; Isel, F. *Colloids Surf. A* **1996**, *112*, 251.
(6) Abrahamsén-Alami, S.; Alami, E.; François, J. *J. Colloid Interface Sci.* **1996**, *179*, 20.
(7) Alami, E.; Almgren, M.; Brown, W.; François, J. *Macromolecules* **1996**, *29*, 2229.
(8) Alami, E.; Almgren, M.; Brown, W. *Macromolecules* **1996**, *29*, 5026.
(9) Chassenieux, C.; Nicolai, T.; Durand, D. *Macromolecules* **1997**, *30*, 4952.

(10) Séréro, Y.; Aznar, R.; Porte, G.; Berret, J. F.; Calvet, D.; Collet, A.; Viguier, M. *Phys. Rev. Lett.* **1998**, *81*, 5584.
(11) Pham, Q. T.; Russel, W. B.; Thibeault, J. C.; Lau, W. *Macromolecules* **1999**, *32*, 2996.
(12) Pham, Q. T.; Russel, W. B.; Thibeault, J. C.; Lau, W. *Macromolecules* **1999**, *32*, 5139.
(13) Hamley, I. W. *Philos. Trans. R. Soc. London A* **2001**, *359*, 1017.
(14) Semenov, A. N.; Joanny, J. F.; Khokhlov A. R. *Macromolecules* **1995**, *28*, 1066.
(15) Berret, J. F.; Séréro, Y.; Winkelman, B.; Calvet, D.; Collet, A.; Viguier, M. *J. Rheol.* **2001**, *45*, 477.
(16) Roovers, J.; Toporowski, P. M.; Douglas, J. *Macromolecules* **1995**, *28*, 7064.
(17) Roovers, J. *Macromolecules* **1994**, *27*, 5359.
(18) Hansen, J. P.; McDonald, I. R. *Theory of Simple Liquids*; Academic Press: San Diego, 1990.
(19) For eample: Klenin, V. J. *Thermodynamics of Systems Containing Flexible-Chain Polymers*; Elsevier: Amsterdam, 1999.
(20) Baxter, J. *J. Chem. Phys.* **1968**, *49*, 2270.
(21) Rao, K.; Srinivasa; Goyal, P. S.; Dasannacharya, B. A.; Menon, S. V. G.; Kelkar, V. K.; Manohar, C.; Mishra, B. K. I *Physica B* **1991**, *174*, 170.
(22) Finnigan, J. A.; Jacobs, D. J. *Chem. Phys. Lett.* **1970**, *6*, 141. Moreels, E.; De Ceuninck, W.; Finney, R. *J. Chem. Phys.* **1987**, *86*, 618.
(23) Maechling-Strasser, C.; François, J.; Clouet, F.; Tripette, C. *Polymer* **1992**, *33*, 627.
(24) Berne, B.; Pecora, R. *Dynamic Light Scattering*; Wiley: New York, 1976.
(25) Loppinet, B.; Stiakakis, E.; Vlassopoulos, D.; Fytas, G.; Roover, J. *Macromolecules* **2001**, *34*, 8216.
(26) Nyström, B.; Walderhaug, H.; Hansen, F. K. *J. Phys. Chem.* **1993**, *97*, 7743.
(27) Johannsson, R.; Chassenieux, C.; Durand, D.; Nicolai, T.; Vanhoorne, P.; Jérôme, R. *Macromolecules* **1995**, *28*, 8504.
(28) For example: Higgins, J. S.; Benoit, K. C. *Polymers and Neutron Scattering*; Brown, W., Ed.; Clarendon Press: Oxford, 1994; *Light Scattering. Principles and Developments*; Clarendon Press: Oxford, 1996.
(29) For example: Mark, J. E.; Erman, B. *Rubberlike Elasticity a Molecular Primer*; John Wiley and Sons: New York, 1988.
(30) Barboy, B. *J. Chem. Phys.* **1974**, *61*, 3194.
(31) Kranendonk, W. G. T.; Frenkel, D. *Mol. Phys.* **1988**, *64*, 403.
(32) Gimel, J. C.; Nicolai, T.; Durand, D. *Eur. Phys. J. E* **2001**, *5*, 415.
(33) Annable, T.; Buscall, R.; Ettelai, R.; Whittlestone, D. *Langmuir* **1994**, *10*, 1065.
(34) Binana-Limbele, W.; Clouet, F.; François, J. *J. Colloid Polym. Sci.* **1993**, *271*, 748.
(35) Kelarakis, A.; Mingvanish, Daniel, C.; Li, H.; Havredaki, V.; Booth, C.; Hamley, I. W.; Ryan, A. J. *Phys. Chem. Chem. Phys.* **2000**, *2*, 2755.
(36) Lobry, L.; Micali, N.; Mallamace, F.; Liao, C.; Chen, S. H. *Phys. Rev. E* **1999**, *60*, 7076.
(37) Filali, M.; Aznar, R.; Svenson, M.; Porte, G.; Appell, J. *J. Phys. Chem. B* **1999**, *103*, 7293. Filali, M.; Michel, E.; Mora, S.; Molino, F.; Porte, G. *Colloids Surf. A* **2001**, *183*, 203.

MA021076D